ELECTRONIC STRUCTURE CALCULATIONS FOR VACANCIES AND OXYGEN-RELATED DEFECTS IN SEMICONDUCTORS

Marko Pesola

Laboratory of Physics
Helsinki University of Technology

Fysiikan laboratorio
Teknillinen korkeakoulu

DISSERTATION 109 (2000)

ELECTRONIC STRUCTURE CALCULATIONS FOR VACANCIES AND OXYGEN-RELATED DEFECTS IN SEMICONDUCTORS

Marko Pesola

Laboratory of Physics
Helsinki University of Technology
Espoo, Finland

Dissertation for the degree of Doctor of Science in Technology to be presented with due permission for public examination and debate in Auditorium K at Helsinki University of Technology (Espoo, Finland) on the 18th of August, 2000, at 12 o'clock noon.

Dissertations of Laboratory of Physics, Helsinki University of Technology
ISSN-1455 1802

Dissertation 109 (2000):
Marko Pesola: Electronic Structure Calculations for Vacancies and Oxygen-Related Defects in Semiconductors
ISBN 951-22-5051-9

OTAMEDIA OY
Espoo 2000

Abstract

Quantum mechanical plane-wave pseudopotential (PWPP) calculations are used to study properties of vacancies and oxygen-related defects in Si and GaAs. Total energies, atomic geometries, charge states, ionization levels, and local vibrational modes for the defects are reported.

The convergence of electronic structure calculations with respect to supercell size is studied for the vacancy (V) and divacancy (V_2) in Si. The negative-U behaviour has been explored in the case of V in Si. The doubly negative charge state of V is shown to have a split structure which can lead to ionization-enhanced diffusion of V. V_2 in Si is shown to have four separate charge states in agreement with experiments. It is found that the neutral (V_2^0) and negative divacancy (V_2^-) have a mixed structure, including both pairing and resonant-bond characters, V_2^0 being more of the pairing type and V_2^- more of the resonant-bond type.

The ionization levels, microscopic structures and local vibration (LV) modes are calculated for vacancy-oxygen (VO) defects in Si. The ionization level for VO is found near the computational conduction band and the charge-state induced shift in the LV frequency is predicted to be upwards as a function of defect level occupation, in agreement with experiments. VO_2 is found to have two degenerate asymmetric stretching modes and thus only one observable mode despite the two oxygen atoms.

The LV frequencies for electrically inert oxygen interstitials (O_i) and oxygen dimers (O_{2i}) are presented. The computed asymmetric stretching frequency of the puckered O_i is found to be slightly underestimated compared to the experimental value. Two competing structures for O_{2i} are found: the staggered O_i-Si-O_i configuration and the skewed O_i-Si-Si-O_i configuration. The changes in the LV frequency spectrum with isotopic substitutions of O are calculated, and the experimental frequencies are shown to originate from the staggered form of O_{2i}. The effects of external pressure on structures and vibrational frequencies are reported.

Various oxygen chain models for thermal double donors (TDDs) in Si are presented. The first three TDDs (TDD0-TDD2) are found to consist of one four-membered ring where two O atoms are bonded to two common Si atoms with one or two adjacent interstitial O atoms. The following TDDs (TDD3-TDD7) are found to consist of similar rings with flanking O_i atoms. The anomalously fast aggregation of oxygen may be explained by the diffusion of these structures. At the later stages shallow donors with a

central "di-Y-lid" core are found to become energetically competitive with the ring structures.

An isolated oxygen atom in GaAs is shown to occupy an interstitial Ga-O-As position and to be electrically inactive. The properties of the substitutional off-centered oxygen in arsenic vacancy (O_{As}) are shown to be at variance with the experimental results. A close similarity of the $(As_{Ga})_2$-O_{As} complex with the experimentally observed Ga-O-Ga defect is found. Especially the negative-U and charge-state induced shifts in local vibrational frequencies are in close agreement with the experiments.

Preface

This thesis has been prepared in the Laboratory of Physics at the Helsinki University of Technology during the years 1996-1999.

I would like to thank my supervisor Academy Professor Risto Nieminen for giving me the opportunity to work in his dynamic research group. I want to thank him for his positive attitude and for providing excellent facilities to conduct computational studies. Most of all, my deepest gratitude is due to Dr. Juhani von Boehm, whose supervision and collaboration has been of crucial importance. In addition, I would like to thank Dr. Tomi Mattila and Dr. Sami Pöykkö for guidance and collaboration. I would also like to thank Professor Martti Puska, Dr. Young Joo Lee, Dr. Markus Kaukonen, Dr. José-Luis Mozos, Mr. Juha Lento, and Mr. Ville Sammalkorpi. The atmosphere in the Laboratory of Physics is genuinely warm and encouraging thanks to colleagues and personnel like Mikko, Andrés, Eira, and Oskari. Dear friends Antti, Heli, Esa, and Elisa have constantly brought joy to the years spend at HUT. My relatives, especially Mom and Dad have always given all the support needed, kiitos äiti ja isä.

I gratefully acknowledge the financial support by the Vilho, Yrjö and Kalle Väisälä Foundation, the Finnish Cultural Foundation, and the Progress of Technology Foundation. The excellent computing resources of the Center for Scientific Computing are also acknowledged.

Finally, I want to thank my dear wife Katja for the love and support during the course of the work.

Espoo, June 2000

Marko Pesola

Contents

Preface iii

List of publications 1

1 Introduction 2

2 Electronic Structure Calculations 4

2.1 Density Functional Theory 4

2.2 Defect formation energies 8

2.3 Calculation of Local Vibrational Modes 9

3 Results 11

3.1 Vacancies and divacancies in silicon 11

3.2 Vacancy-oxygen defects in silicon 16

3.3 Interstitial oxygen complexes in silicon 18

3.4 Structures of thermal double donors in silicon 20

3.5 Oxygen-related defects in GaAs 24

4 Summary 28

References 28

List of publications

This thesis consists of an overview and the following publications:

I. M. J. Puska, S. Pöykkö, M. Pesola, and R. M. Nieminen, Convergence of supercell calculations for point defects in semiconductors: Vacancy in silicon, Physical Review B **58**, 1318-1325 (1998).

II. M. Pesola, J. von Boehm, S. Pöykkö, and R. M. Nieminen, Spin-density study of the silicon divacancy, Physical Review B **58**, 1106-1109 (1998).

III. M. Pesola, J. von Boehm, T. Mattila, and R. M. Nieminen, Computational study of interstitial oxygen and vacancy-oxygen complexes in silicon, Physical Review B **60**, 11449-11463 (1999).

IV. M. Pesola, J. von Boehm, and R. M. Nieminen, Vibrations of the interstitial oxygen pairs in silicon, Physical Review Letters **82**, 4022-4025 (1999).

V. M. Pesola, Y. J. Lee, J. von Boehm, M. Kaukonen, and R. M. Nieminen, Structures of thermal double donors in silicon, Physical Review Letters **84**, 5343-5346 (2000).

VI. M. Pesola, J. von Boehm, V. Sammalkorpi, T. Mattila, and R. M. Nieminen, Microscopic structure of oxygen defects in gallium arsenide, Physical Review B **60**, R16267-R16270 (1999).

The author has had an active role in all phases of the research reported in this thesis. He has been involved in the planning of the calculations, the development of the computer programs, and the interpretation of the results. The author has written the first versions of Publications II-VI and contributed to the writing of Publication I. He is responsible for all calculations presented in Publications II-IV and most of the calculations in Publications V and VI. He has actively taken part in the planning and performing of the calculations reported in Publication I.

1 Introduction

The most important method to grow bulk Si and also GaAs is the Czochralski (Cz) method. In this method a crystal ingot is pulled from the melt held in a rotating quartz crucible. As a byproduct of this process oxygen is incorporated into the crystal lattice.

Oxygen in Cz-Si is supersaturated and inhomogeneously distributed with a concentration of the order of 10^{18} cm^{-3}. Therefore heat treatments are used to homogenize the oxygen distribution. At elevated temperatures oxygen complexes dissociate and a high concentration of interstitial oxygen (O_i) forms. At annealing temperatures higher than 350°C, O_is start to diffuse and cluster exhibiting donor character form. As a first step in clustering, single O_is bind to interstitial dimers O_{2i}, which have a decisive role in the donor formation process [1–3]. There are several families of thermal donors in Si, their existence depending on the annealing temperature [4–7]. The most important ones from the technological point of view are the thermal double donors (TDDs) [4,5]. Unfortunately, performing electronic structure calculations for the TDDs is difficult because the highest occupied electronic state is spatially extended [5] and the TDD core structure consisting of oxygen atoms is larger than the supercell sizes typically used in electronic structure calculations. This has hindered electronic structure calculations related to TDDs.

Ion implantation is a widely used technique for the introduction of dopants into semiconductors. Doping of semiconductors with foreign atoms leads to changes in the electronic character of the semiconductor: it can have an excess of electrons (n type semiconductor) or an excess of holes (p type semiconductor). As a byproduct of ion implantation interstitial-vacancy - pairs are produced. The vacancy (V) in bulk Si is the simplest example of a native point defect in a semiconductor lattice. Vacancies have an important role, e.g., in point-defect mediated diffusion and therefore the knowledge of the ionic and electronic structures of V is important. Experimentally, vacancies in Si have successfully been monitored using the electron paramagnetic resonance (EPR) technique [8]. Despite of its importance the theoretical description of V in Si has been turned out to be a difficult task.

The divacancy (V_2) in Si is attractive from the theoretical point of view because it has been identified by means of EPR and many of its properties are known. Early EPR measurements and linear-combination-of-atomic-orbitals (LCAO) models give a pairing mode relaxation for both positive

and negative charge states of V_2 [9]. The pairing mode relaxation of V_2^- was later questioned by Saito and Oshiyama [10].

Annealing of irradiated silicon produces off-site substitutional vacancy-oxygen pairs (VO) and more complicated oxygen-related defects. VO is the famous A center with an ionization level at $E_c - 0.17$ eV (E_c denotes the conduction band minimum) [11, 12]. The structure of VO^- has been determined experimentally already in the sixties [11, 12] and therefore it is suitable for testing computational methods.

GaAs is the most important compound semiconductor. Especially it is used in applications requiring high performance and fast electronics. GaAs crystals can be grown with a variant of the Czochralski method, called the liquid encapsulated Czochralski (LEC) method. In this method liquid GaAs is held in a quartz crucible and there is considerable amount of oxygen present in the as-grown crystal. The structure of oxygen defects in GaAs has so far been assumed to resemble the ones in Si.

In this thesis, defects in semiconductors are studied using *ab initio* calculations. In Publication I, V in Si is studied as a test case for the convergence of the electronic structure calculations. In Publication II, a spin-density study of the V_2 is carried out. Publication III contains a systematic study of oxygen-related defects in Si. Publication IV is a computational study of the vibrational properties of oxygen dimers in Si. Publication V contains a systematical study of the structures of the thermal double donors in Si. In Publication VI, the Ga-O-Ga defect structure in GaAs is reported. The summary part of the thesis contains also novel complementary results which were not included in Publications I-VI.

The summary part of this thesis is organized as follows. The computational methods are reviewed in Section 2. The results obtained are reviewed in Section 3. A brief summary is given in Section 4.

2 Electronic Structure Calculations

The fundamental problem of computational solid state physics is the solution of the many-body Schrödinger equation for a system containing interacting electrons and ions. Usually the time scale of electrons is several orders of magnitude smaller than the ionic time scale and therefore it can be assumed that the electrons adapt instantaneously the current ionic positions. In this Born-Oppenheimer approximation electrons follow adiabatically the movements of the ions. Even with this approximation the problem is still far too complicated to be solved in the actual solid state environment. In 1964 Hohenberg and Kohn [13] and in 1965 Kohn and Sham [14] introduced the density-functional theory (DFT) that reduces the problem to the effective one-electron problem. During the last decades there have been numerous successful applications of DFT to solid state problems. Combined with the Hellmann-Feynman theorem [15], DFT forms an efficient method to study electronic, structural and dynamic properties of matter.

2.1 Density Functional Theory

The Kohn-Sham total-energy functional for a general electron-ion system is written as follows (Hartree atomic units are used throughout):

$$\begin{aligned} E_{\text{tot}}[\{\psi_{i\sigma}(\mathbf{r})\},\{\mathbf{R}_\alpha\}] &= \sum_{i,\sigma} f_{i\sigma}\left\langle \psi_{i\sigma}(\mathbf{r})\left|-\frac{1}{2}\nabla^2\right|\psi_{i\sigma}(\mathbf{r})\right\rangle \\ &+ \frac{1}{2}\int\int\frac{n(\mathbf{r})n(\mathbf{r}')}{|\mathbf{r}-\mathbf{r}'|}d\mathbf{r}d\mathbf{r}' \\ &+ \int V_{\text{ion}}(\mathbf{r})n(\mathbf{r})d\mathbf{r} + \frac{1}{2}\sum_{\alpha,\beta,\alpha\neq\beta}\frac{Z_\alpha Z_\beta}{|\mathbf{R}_\alpha-\mathbf{R}_\beta|} \\ &+ E_{\text{xc}}[n_\uparrow(\mathbf{r}),n_\downarrow(\mathbf{r})]. \end{aligned} \tag{1}$$

This total energy functional depends on the positions of atoms $\mathbf{R}_\alpha$ and the single particle Kohn-Sham spin-orbitals $\psi_{i\sigma}$ only. The first term is the kinetic energy of non-interacting electrons where the summation runs over all spin-orbitals (i for orbital and σ for spin) and the occupation number $f_{i\sigma}$ gets values 0 or 1. The electron density is calculated from the single particle Kohn-Sham spin-orbitals

$$n(\mathbf{r}) = \sum_{i,\sigma} f_{i\sigma}|\psi_{i\sigma}(\mathbf{r})|^2. \tag{2}$$

The second term in Eq. (1) is the Hartree energy, the energy term arising from the electrostatic electron-electron interaction. The third term is the interaction energy of the electron density in the potential V_{ion} created by the ions. The fourth term describes the ion-ion interaction of ions with point charges Z_α and Z_β. The last term is the exchange-correlation energy. All quantum mechanical many-body effects are buried in this term which then contains approximations made forming the Kohn-Sham total energy functional. The exact form of E_{xc} is not known. The most widely used approximation is the local spin-density approximation (LSDA), where the exchange-correlation energy is approximated by the exchange-correlation energy of the uniform electron gas

$$E_{\text{xc}}[n_\uparrow(\mathbf{r}), n_\downarrow(\mathbf{r})] = \int \epsilon_{\text{hom}}(n_\uparrow(\mathbf{r}), n_\downarrow(\mathbf{r}))n(\mathbf{r})d\mathbf{r}, \tag{3}$$

where ϵ_{hom} is the exchange-correlation energy density of the homogeneous electron gas and $n_\uparrow$ and $n_\downarrow$ are the densities of spin-up and spin-down electrons, respectively. The use of E_{xc} of the homogeneous electron gas was originally proposed by Kohn and Sham [14] in the non-spin-polarized form and later augmented to this spin-polarized case by Gunnarsson and Lundqvist [16]. For practical use in DFT, ϵ_{hom} has been calculated by the Monte Carlo methods [17] and has several parametrisations [18, 19]. Regardless of their simplicity LSDA and the non-spin-polarized local density approximation (LDA) [obtained by setting $n_\uparrow(\mathbf{r})$-$n_\downarrow(\mathbf{r})$=0] have been successfully used in calculations during past decades. Especially structural properties are obtained in agreement (with the known exceptions, e.g., too small bond lengths for molecules) with experiments. When applied to semiconductors, the most severe deficiency of LDA is the size of the forbidden energy gap. For example, the size of the calculated Si bandgap based on Kohn-Sham one-electron states is approximately one half of the experimental value, only 0.6 eV. This influences the ionization levels (to be discussed below), especially in the upper part of the energy gap. Another LDA-related feature is the underestimation of the lattice constant and too large cohesive energy for solids. This leads usually to overestimation of the local vibration (LV) frequencies by a few percents.

Several attempts have been made to improve LDA. These include generalized gradient approximations (GGA) [20], local mass approximation (LMA) [21], and screened non-local exchange potential (sX-LDA) [22]. None of these have succeeded in correcting all errors and still being useful in large-scale electronic structure calculations.

Taking the functional derivative of Eq. (1) with respect to $\psi_{i\sigma}^*$ results in the Kohn-Sham equation for $\psi_{i\sigma}$ [23]

$$\left(-\frac{1}{2}\nabla^2 + V_{\text{eff}}^{\sigma}\right)\psi_{i\sigma}(\mathbf{r}) = \epsilon_{i\sigma}\psi_{i\sigma}(\mathbf{r}). \tag{4}$$

Eq. (4) is an effective single-particle Schrödinger equation that has exactly the same form as the Schrödinger equation for the non-interacting electrons in an external potential. Here, the effective potential is

$$V_{\text{eff}}^{\sigma} = V_{\text{H}} + V_{\text{ion}} + V_{\text{xc}}^{\sigma}, \tag{5}$$

where V_{xc}^{σ} is a functional derivative of the exchange-correlation energy with respect to the spin density (n_σ) and V_{H} is the electrostatic potential due to electrons.

The effective potential depends on the electron density, which in turn depends on the spin-orbitals. Therefore the Kohn-Sham equations should be solved in a self-consistent manner. After every update of spin-orbitals, the corresponding electron density and the effective potential are to be calculated. The corresponding new Hamiltonian then operates on the spin-orbitals and so on. This should be continued until the total energy and the spin-orbitals do not change more than a preset limit.

The Born-Oppenheimer approximation allows the ionic positions to be treated as a set of parameters in Eq. (1). The Hellmann-Feynman theorem used in the computational studies states that the forces on ions can be calculated as derivatives of Eq. (1) solely with respect to ionic positions [15]:

$$\mathbf{F}_\alpha = -\frac{\partial E_{\text{tot}}}{\partial \mathbf{R}_\alpha}. \tag{6}$$

According to the Hellmann-Feynman theorem the calculation of the ionic forces reduces to the calculation of the derivative of the electrostatic energy of the ion with respect to **R**. Hellmann-Feynman forces can then be used in relaxing the ionic coordinates, obtaining the second derivatives for the LV calculation or taking the next ionic step in molecular dynamics.

In this work plane-waves are used as basis functions to form $\psi_{i\sigma}$'s. This is a natural choice, if combined with the periodic boundary conditions and the supercell approximation. Plane-waves form a complete set that is simple and unbiased. The completeness means that an arbitrary accuracy can be obtained by increasing the number of plane-waves. Hellmann-Feynman

forces are easy to calculate for plane-waves because they do not depend on the ionic positions. It is especially important for calculations that the fast Fourier transform (FFT) can be used in switching between the real and reciprocal spaces. This facilitates the calculations because some of the energy terms are more easily calculated in the real and others in the reciprocal space.

Inner electrons that have low eigenvalues (for example 1s, 2s, 2p and 3s in Si) are not affected by the chemical bonding which is basically due to the valence electrons. Therefore it is not necessary to describe the former explicitly in the calculations. By combining the ionic potential of the form Z/r with the potential of the inner electrons in the pseudopotential decreases the computational burden significantly. First of all, the number of electrons (states) drops, because only 4 of 14 electrons in the Si atom need to be treated as valence electrons. Second, the steep nature of the wavefunctions of inner (or core) electrons would require huge kinetic energy cut-offs for the plane-wave basis. Smoothing of the potential removes wiggles from the valence wavefunctions and reduces the number of the plane-waves needed to describe the wavefunctions.

Pseudopotentials are typically constructed for atoms and then applied to solid state problems. The construction scheme can preserve the original electron density inside some set radius, thus the method is norm-conserving [24–27], or this requirement can be relaxed leading to a non-norm-conserving or ultrasoft Vanderbilt pseudopotentials [28]. In this work norm-conserving pseudopotentials are used for Si, Ga, and As, while ultrasoft Vanderbilt pseudopotentials are used for O.

The special **k**-point sampling schemes can be used for the Brillouin zone integrations. In this work the Monkhorst-Pack or uniform sampling [29], the Makov-Shah **k**-points that minimize the defect-defect interaction [30], and simple Γ-point samplings are used.

Use of the periodic supercells to describe isolated point defects requires supercells which are large enough to prevent spurious interactions between the defects in the adjacent supercells. These interactions can be mechanical (elastic) or electronic. Elastic interaction between the defect replicas hinders the relaxation of the defect ionic structure. The electronic interaction manifests itself in the dispersion of the defect levels in the supercell. This means that the eigenvalues depend on the position in the **k**-space, which can lead to the hybridization of the delocalized Bloch states and the localized defect states.

Makov and Payne [31] discussed the correction of spurious Madelung-type interactions of charged defects with their periodic replicas in solids in supercell calculations. Using their theory the correction is estimated to be of the order of 0.1 eV and 0.2-0.3 eV, for singly positive or negative and doubly positive or negative charge states, respectively, when a 64 atom-site supercell is used [32].

2.2 Defect formation energies

The energy required to form a defect in an otherwise perfect crystal is the formation free energy ($\Omega_f = E_f - TS$). The entropy term can be approximated to be constant, i.e. it does not change significantly between different charge states of the defect. Thus, the ionization level positions can be obtained based on E_f, only. For the thermodynamical concentration of a defect the entropy term is essential. It contains both the configurational entropy of a defect population and the local defect entropy, due to changes in the vibrational degrees of freedom. The formation energy of a defect in the charge state Q is given by [33–36]

$$E_f(Q) = E_{\text{tot}}(Q) + Q(E_v + \mu_e) - \sum_s n_s \mu_s, \tag{7}$$

where Q is the charge of the defect in units of the elementary charge, E_v is the valence band maximum and μ_e is the electron chemical potential relative to the valence band maximum. The constituents of the last summation, n_s and μ_s are the number of the s type atoms in the supercell and the atom chemical potential, respectively.

The values for the valence band maximum and the host atom chemical potential are obtained from a defect-free bulk calculation by using the same computational approximations as the defect calculations.

In the case of a compound semiconductor such as GaAs the atomic chemical potentials are constrained by the equation

$$\mu_{\text{Ga}} + \mu_{\text{As}} = \mu_{\text{GaAs}}^{\text{bulk}}. \tag{8}$$

$\mu_{\text{GaAs}}^{\text{bulk}}$ can be obtained from the total energy of the defect-free GaAs bulk, but μ_{Ga} and μ_{As} are determined by the growth conditions. Setting μ_{As} equal to the elemental value (from rhombohedral arsenic), so that the μ_{Ga}

is determined from the equation above, describes the As-rich growth conditions. The heat of formation (ΔH) for GaAs determines the range where the energies can vary:

$$\Delta H = \mu_{\mathrm{Ga(bulk)}} + \mu_{\mathrm{As(bulk)}} - \mu_{\mathrm{GaAs}}^{\mathrm{bulk}}, \tag{9}$$

where $\mu_{\mathrm{Ga(bulk)}}$ and $\mu_{\mathrm{As(bulk)}}$ are the values for the elemental Ga and As bulk.

The low temperature form of SiO_2, α-quartz, is used to obtain the chemical potential of an oxygen atom in Si. Similarly, in the case of oxygen defects in GaAs, the chemical potential for oxygen should be calculated from some relevant compound. The compound used in this work is Ga_2O_3.

After determining the chemical potentials, Eq. (7) can be applied to obtain the *ionization levels* and formation energies for the defects. The ionization levels mark the electron chemical potential values which change the charge state of the defect to another with lower formation energy according to Eq. (7). The binding energy of the system can also be calculated with the help of the formation energies. For example the binding energy of oxygen dimer is

$$E_b = 2E_f(\mathrm{O_i}) - E_f(\mathrm{O_{2i}}). \tag{10}$$

The valence band maximum E_v has been corrected using the average potential correction [36] as

$$E_v = E_v(\mathrm{bulk}) + \left(V_{ave}(\mathrm{defect}) - V_{ave}(\mathrm{bulk})\right). \tag{11}$$

The average potential correction is needed because of the limited supercell size. At the boundary of the supercell ("far" away from the defect) the difference in the average potential of the defect calculation and corresponding bulk calculation reflects the supercell size effect. Basically this correction aligns the energies so that comparison between different charge states can be made.

2.3 Calculation of Local Vibrational Modes

For the calculation of the LV modes of a defect it is sufficient to consider only a single supercell. This is because the interaction between the defect replicas is neglibly small and has only a minor effect on the localized vibrations of a defect [37]. In contrast, the phonon density of states can not

be obtained without properly dealing with the periodicity. The total energy of a supercell can be written as a Taylor series around the equilibrium positions of ions $\mathbf{R}_\alpha$,

$$\begin{aligned} E_{\mathrm{tot}}(\{R_{\alpha i}+s_{\alpha i}\}) &= E_{\mathrm{tot}}(\{R_{\alpha i}\}) \\ &+ \frac{1}{2}\sum_{\substack{\alpha i \\ \beta j}} \frac{\partial^2 E_{\mathrm{tot}}}{\partial R_{\alpha i}\partial R_{\beta j}} s_{\alpha i} s_{\beta j} + ... \end{aligned} \qquad (12)$$

where $s_{\alpha i}$ is the i'th Cartesian component of the atomic displacement of the ion α. Neglecting higher order terms leads to the *harmonic approximation* used here.

The derivatives of the total energy in Eq. (12) are called the coupling constants

$$\Phi_{\alpha i}^{\beta j} \equiv \frac{\partial}{\partial R_{\alpha i}}\left(\frac{\partial E_{\mathrm{tot}}}{\partial R_{\beta j}}\right). \qquad (13)$$

They are obtained as numerical derivatives of the Hellmann-Feynman forces in this work.

Using the standard method of substituting the normal mode trial solution

$$s_{\alpha i} = \frac{1}{\sqrt{M_\alpha}} u_{\alpha i} e^{i\omega t} \qquad (14)$$

to the ionic equations of motion, the frequencies and amplitudes of the displacements can be solved. The substitution results in the equations

$$-\omega^2 u_{\alpha i} + \sum_{\beta j} D_{\alpha i}^{\beta j} u_{\beta j} = 0, \qquad (15)$$

where $D_{\alpha i}^{\beta j}$ is defined as the dynamical matrix

$$D_{\alpha i}^{\beta j} \equiv \frac{1}{\sqrt{M_\alpha M_\beta}} \Phi_{\alpha i}^{\beta j}. \qquad (16)$$

In practice the LV mode calculations are done using the following procedure. Selected atoms in the supercell are displaced to all three Cartesian directions. After each displacement electronic structure for this configuration is optimized and the resulting Hellmann-Feynman forces are calculated. This is done for all atoms which were *a priori* considered important for the

description of the local modes of the defect. The dynamical matrix is then calculated by finite differences using these forces and displacements. The normal modes and the corresponding vibrational frequencies can then be obtained by diagonalizing the dynamical matrix [38].

The motion of the ions can be directly simulated with *ab initio* molecular dynamics (MD). In the MD simulation the simulation time has to be chosen so long that all relevant vibration modes have evolved several periods. If the defect includes some light element, like oxygen, the highest LVs have high enough frequency to be distinguished from the host lattice vibrations. The frequency of this vibration mode can then be obtained from the power spectrum of the velocity or position autocorrelation function of the ionic coordinates [39]. These two methods produce similar frequencies, but with the dynamical matrix method, also the normal modes are obtained.

It was found for the small 32 atom-site supercell that the interactions between the localized modes of the defect in the central supercell and the periodic replicas are insignificant. This was tested by taking a large supercell and different numbers of atoms around the defect into account in the calculations. It turned out that in describing the localized modes such as the asymmetric stretching mode of the vacancy-oxygen defect in Si only a very limited number of atoms are needed [37]. More crucial for the calculation is the convergence of the forces when the defect ionic structure is optimized. The resultant ionic forces should be of the order of 0.5 meV/Å, if accuracy of a few cm^{-1} is required in the calculated LV frequencies. Another important point is the convergence of the electronic structure in the actual LV mode calculations. As a basic rule, the atom-shift-induced force should be at least 100 times larger than the forces on other atoms that are far away from the ion considered.

3 Results

3.1 Vacancies and divacancies in silicon

In Publications I and II the convergence of the supercell calculations for the vacancy (V) and divacancy (V_2) in Si has been studied. The ionic relaxations, defect formation energies, and ionization levels have been calculated with several different supercell sizes and **k**-point meshes. Figure 1 shows the convergence of formation energies and point group symmetries for the

neutral V and V_2. As can be seen, the convergence is slow for V and a 216 atom-site supercell is required to obtain the final D_{2d} symmetry (see Fig. 2 for the relaxation modes of the monovacancy). In the case of V_2 the symmetry obtained in calculations is S_2 with all supercells and the main difference is in different relaxation modes that all preserve the S_2 point group symmetry (see Fig. 3).

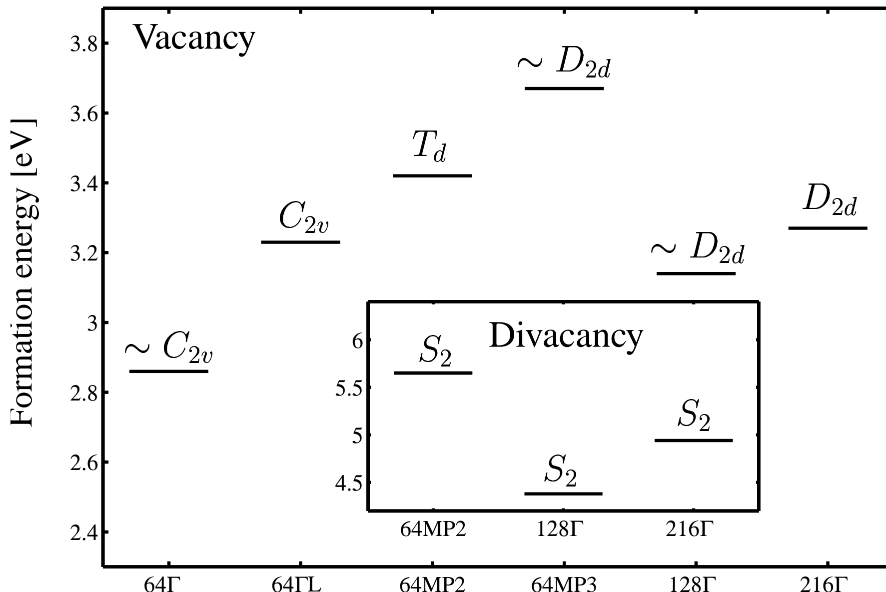

Figure 1: Formation energies E_f and point group symmetries for the neutral vacancy and divacancy in Si. Schematic figures of the symmetries of the relaxation modes are given in Figs. 2 and 3. Integers on the x-axis denote the numbers of atom sites in the supercell. MP2 and MP3 denote Monkhorst-Pack 2^3 and 3^3 **k**-point samplings used.

Figure 4 shows the ionization levels for both V and V_2 obtained by solving μ_e from the equation $E_f(Q) = E_f(Q')$ using different supercells and **k**-point samplings. Monkhorst-Pack (MP) **k**-point meshes give T_d symmetries for positive and neutral charge states and no negative-U effect[1]. This is in disagreement with the negative-U property of V that has been the-

[1] U is the energy change when a electron is placed on the highest energy orbital occupied by one electron. If U is negative, the Coulombic repulsion energy between electrons is exceeded by the energy obtained by ionic relaxation [40–42].

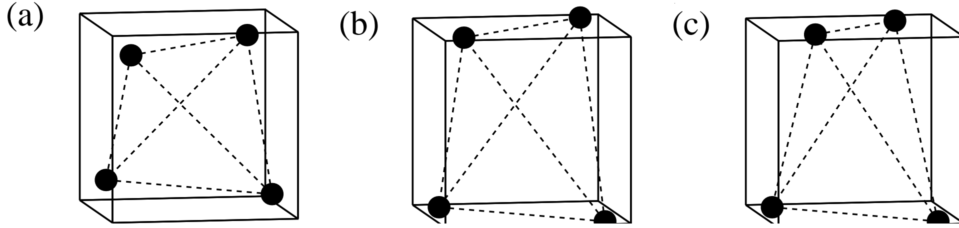

Figure 2: Relaxation modes for a vacancy in silicon. a) Breathing mode with symmetry T_d. b) Two short and four long bonds: D_{2d}. c) Two short, unequal and four equal long bonds: C_{2v}.

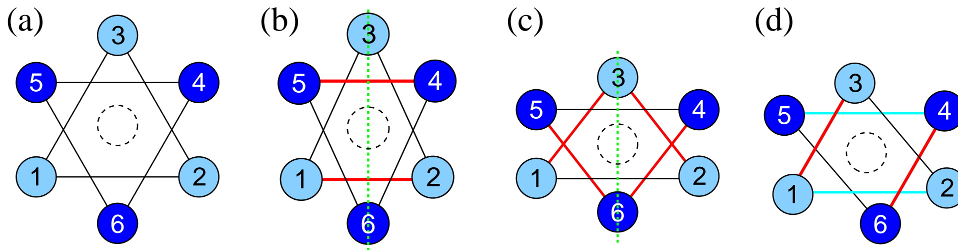

Figure 3: Relaxation modes for divacancy in silicon. a) Ideal V_2. b) Pairing mode (C_{2h}). c) Resonant-bond mode (C_{2h}). d) Mixed mode (S_2).

oretically predicted by Baraff *et al.* [43] and experimentally confirmed by Watkins and Troxell [8]. The reason for this discrepancy is the hybridization of the defect state with the valence band states due to the dispersion in one-electron states and MP **k**-point sampling. In contrast to these MP results, all Γ-point calculations give correctly a negative-U effect: the singly positive charge state is thermodynamically metastable in agreement with the experiments [8]. Recently Öğüt *et al.* [44] studied V by the cluster method. Their results are in close agreement with the results obtained here using largest 216 atom-site supercell.

The negative charge states of V behave in a complex way (Fig. 4). The calculations with the MP **k**-points give all three charge states 0, - and 2-, but the Γ-point approximation results in the case of 64 and 216 atom-site supercells in another negative-U phenomenon, now the singly negative charge state being thermodynamically metastable. In the case of singly and doubly negative charge states the calculations with the supercell of 216

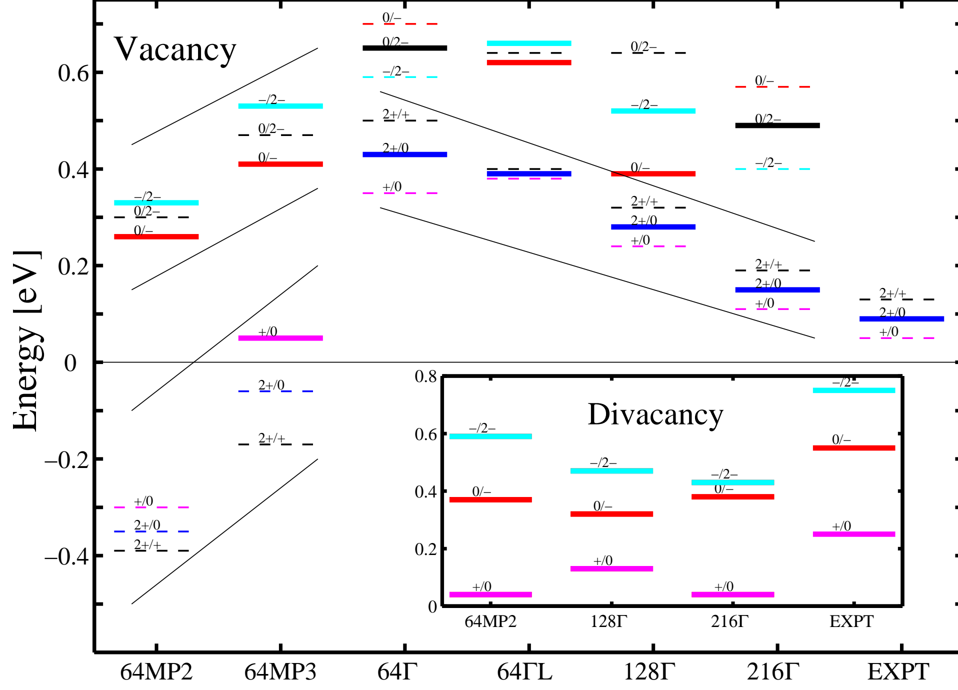

Figure 4: Ionization levels of vacancy and divacancy in silicon. Solid lines represent the positions of ionization levels. The valence band top is located at the zero energy.

atomic sites and the Γ-point sampling result in an ion configuration of a split vacancy shown in Fig. 5(a). In this configuration one of the nearest-neighbor Si atoms has moved halfway towards the center of the vacancy resulting in the D_{3d} point symmetry, that is, the symmetry of an ideal divacancy. The split-vacancy geometry has been suggested for the doubly negative vacancy by Corbett and Bourgoin [45]. The stability of the configuration arises from the reduced electron repulsion, because in the split configuration the deep level electrons are localized over six dangling bonds. The split-vacancy is the saddle point for the vacancy migration. Therefore, the charge state change can result in a migration of the vacancy through silicon lattice without thermal activation over a barrier.

In Publication II it was found that the computed formation and binding energies and ionization levels of V_2 converge nicely as a function of the supercell size (Fig. 4). Ionization level positions are slightly underestimated

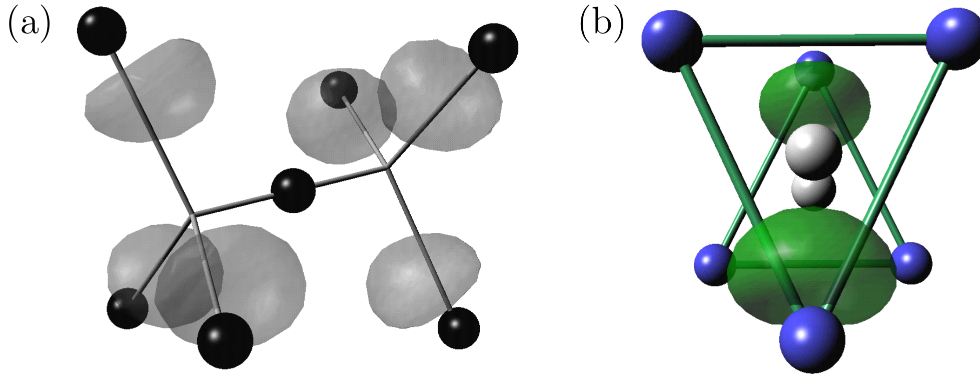

Figure 5: a) The split configuration of doubly negative Si vacancy. b) Uppermost occupied electronic state of V_2^+. The unpaired electron is located opposite to the short bonds. The defect has an approximative C_{2h} symmetry.

and the binding energy of V_2 is in close agreement with experiments. However, the resulting atomic geometries show a large scatter depending on the approximations used. It was found that using the largest 216 atom-site supercell results in a mixed structure of the S_2 symmetry for the positively charged, neutral and negatively charged divacancies. The structures of the positive and neutral divacancies are of the pairing type whereas the negatively charged divacancy is of the resonant-bond type. Figure 3 shows the different relaxation modes for V_2. The resonant mode relaxation for V_2^- was originally found by Saito and Oshiyama in their DFT supercell calculations using a 64 atom-site supercell [10]. Watkins and Corbett, interpreting their EPR experiments using an LCAO-model concluded that both singly positive and negative divacancies experience pairing type relaxations with point group symmetry C_{2h} [9] [See Fig. 3(b)]. According to their results the uppermost occupied electronic state has a non-vanishing density on the mirror plane [dashed line in Fig. 3(b)]. This was explained to be a result of a large Jahn-Teller distortion that changes the order of defect levels in the forbidden energy gap.

Figure 5(b) shows the uppermost occupied electronic state for the singly positive charge state of V_2. In the case of V_2^+ the uppermost occupied electronic state has a non-vanishing electronic density on the mirror plane and the deviation from the C_{2h} symmetry is small.

In the case of the singly negative V_2, the mixed relaxation pattern is found

with a resonant bond character [Fig. 3(c)]. Recently Öğüt and Chelikowsky found based on their large cluster calculations that the relaxation mode of V_2^- is due to a large Jahn-Teller distortion [46]. The changes on the structure of V_2 are highly anisotropic in nature. Even the largest supercell of 216 atom-sites used in Publication II is not large enough in the $[1\bar{1}0]$ direction to allow proper relaxations.

3.2 Vacancy-oxygen defects in silicon

Electron and ion implantation produces Frenkel pairs consisting of Si interstitial (I) and V. Most of these pairs recombine and only a small fraction survives. V and I are mobile at room temperature and are known to contribute to the self-diffusion in Si significantly. Their migration can be interrupted by recombination, agglomeration into defect clusters such as V_2, and by interaction with impurities and dopant atoms. Experiments have shown that vacancies form pairs with interstitial oxygen and phosphorus, while interstitials replace carbon and boron atoms in the substitutional sites [47]. VO is observed in all electrical and optical studies irrespective of the type of the irradiation used. VO has an acceptor level (0/-) near the conduction band minimum [48–50]. The structure of the negatively charged VO has been established by EPR measurements [11, 12], and LVM studies have shown that the structure of the neutral defect deviates only marginally from this [51]. The diffusion barrier for VO is low, 1.4-1.8 eV compared to 2.53 eV for O_i [52, 53].

Table 1 shows the calculated and experimental frequencies related to VO and other complexes studied in Publication III. The calculated asymmetric stretching frequencies of neutral defects are overestimated (probably due to the LDA overestimation of the bonds) but the isotopic shifts are in excellent agreement with the experimental values. A larger difference is found in the charge-state induced shift of the asymmetric stretching mode for VO. The calculated value is only 7 cm^{-1} while the experimental value is 50 cm^{-1}. The reason for this is probably related to the insufficient relaxations due to the small 32 atom-site supercell used in the calculations. The acceptor level is found 0.4 eV above valence band top near the calculated conduction band minimum, in qualitative agreement with the experiments.

It is interesting to note that the highest LV frequencies of VO complexes are generally lower than those measured for the thermal donors. Therefore bare VO complexes are not suitable thermal donor candidates. They should

Table 1: Asymmetric stretching mode frequencies for VO, VO_2, and V_2O. The isotopic shifts ($^{16}O \rightarrow {}^{18}O$) are given in parentheses.

	VO	$[VO]^-$	VO_2	V_2O
Calculations:	843 (37)	850	912 (41)	829
Experiments:	835[a] (37)[b]	885[a]	895[c] (39)[d]	-

[a]Ref. [51], [b]Ref. [54], [c]Ref. [55], [d]Ref. [56],

have flanking interstitial oxygen atoms that could generate higher LV frequencies. It should also be noted that VO complexes studied in Publication III are not shallow donors but acceptors.

The possibility of silicon interstitial (I) ejection can be studied with the formation and binding energies. The calculated energy gain when I and V recombine is several electron volts. This is reflected also to the process where I recombines with VO complexes. In the case of VO the reaction is:

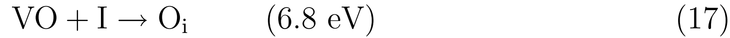

$$VO + I \rightarrow O_i \qquad (6.8\ \text{eV}) \tag{17}$$

and with VO_2

$$VO_2 + I \rightarrow O_{2i} \qquad (5.9\ \text{eV}). \tag{18}$$

Thus it is not likely that I's would be ejected from small O_i chains. However, the binding energy drops rapidly with increasing chain size and I ejection may take place in the case of the larger O_i chains.

In the annealing of VO and V_2 second order defects such as V_2O and VO_2 are formed. The symmetry of VO_2 was found to be D_{2d} and the normal modes of the oxygen atoms in the asymmetric stretching mode are orthogonal and decoupled. This leads to a degenerate asymmetric stretching mode with a slightly higher frequency than the corresponding frequency of VO.

V_2O is shown to have a high-spin (S=1) state 0.18 eV higher than the spin-compensated state in agreement with the experiments [57]. The ionization level associated to this complex is found to lie 0.34 eV above the valence band top. The highest vibrational frequency of V_2O is lower than the corresponding frequencies of VO and VO_2.

3.3 Interstitial oxygen complexes in silicon

Isolated interstitial oxygen (O_i) is the dominant form of oxygen in Cz-Si after the homogenizing heat treatments. As a fingerprint of O_i, infrared (IR) absorption spectra show a peak related to the Si-O-Si at 1106 cm^{-1} and 1136 cm^{-1} at room temperature and the low temperatures, respectively [58–60]. The large temperature shift may indicate possible anharmonicities. No other known oxygen-related defect exhibits such a large shift in the LV frequency. In Publication III it was found that the structure of O_i is bond-centered with oxygen atom displaced slightly from the actual bond center forming a puckered structure. The bond center barrier is small (20 meV) but nonzero. The upper panel in Fig. 6(a) shows the calculated and experimental frequencies related to O_i. The calculated asymmetric stretching frequency of 1098 cm^{-1} is slightly below the experimental value. This and the other differences between the calculations and experiments may be a reflection of the anharmonicity of O_i. In Publication III a qualitative agreement in the pressure coefficient of the asymmetric stretching vibration mode was found: the frequency drops when the external hydrostatic pressure in the supercell was risen, in agreement with the experiments [61].

O_is become mobile at temperatures larger than 350°C and begin to agglomerate and form first oxygen dimers. In Publications III and IV two electrically inactive O_{2i} structures were studied. The staggered Si-O_i-Si-O_i-Si and skewed Si-O_i-Si-Si-O_i-Si structures are nearly degenerate in energy and were found to have binding energies of 0.2 and 0.1 eV, respectively. The lower panel of Fig. 6(a) shows the calculated LV frequencies for the two dimer structures and positions of experimentally measured peaks [3,62,63]. As can be seen the experimental frequencies of O_{2i} at 1060, 1012, 690, and 556 cm^{-1} are most naturally associated with the staggered O_{2i}. The experimental frequency of O_{2i} at 1105 cm^{-1} is found to originate from the skewed configuration of O_{2i}.

Figure 6(b) shows the LV frequencies of different isotope configurations of O_{2i}. The calculated LV frequencies for the staggered dimer and their isotopic shifts agree closely with the experimental values, whereas those for the skewed dimer show considerable differences.

The differences in the LVs for the two dimer structures can be explained with the variation of the strength of interaction between the oxygen atoms. Closely placed O_is cause larger splittings in the LV frequencies due to their

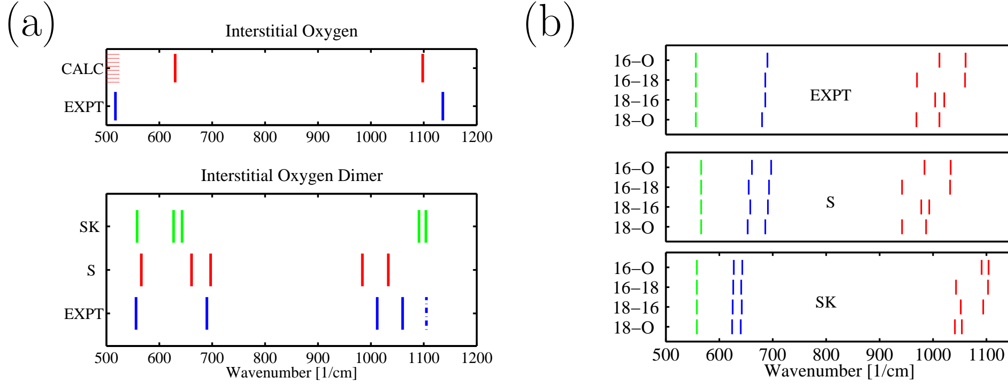

Figure 6: a) Local vibration frequencies for O_i and O_{2i}. CALC, EXPT, SK, and S denote our calculations, experiments from Refs. [3, 59, 62, 63], (calculated) skewed O_i-Si-Si-O_i and staggered configurations, respectively. The experimental dash-dotted bar in the lower panel belongs to a different configuration than the solid bars. b) LV frequencies for O_{2i} with different O isotopes. The uppermost panel shows the experimental frequencies [3, 62], the middle panel shows the frequencies for the staggered O_{2i} and the lowest panel shows the vibration frequencies of the skewed O_i-Si-Si-O_i.

mutual interaction. In the skewed configuration the oxygen atoms are separated by two silicon atoms whereas in the staggered configuration only by one silicon atom. Thus oxygen atoms have a stronger interaction in the latter case [see the lower panel of Fig. 6(a)].

In Publication V the lowest energy configurations for the electrically inert O_{3i} and O_{4i} were calculated. The configurations turned out to be staggered $[1\bar{1}0]$ chains. Table 2 shows the formation and binding energies for the first five electrically inactive complexes. The formation energy per oxygen atom drops when the oxygen cluster size increases. Therefore the binding energy of a single oxygen in a cluster increases with increasing cluster size. Thus it can be concluded that during annealing and in the TDD growth process O_{ni} chains form and should also be observed in IR experiments. The LV calculation for the staggered O_{3i} gives a triplet of asymmetric stretching frequencies at 984, 947, and 900 cm^{-1} below the corresponding O_{2i} doublet at 1033 and 984 cm^{-1}. Therefore this frequency of O_{3i} may be related to the 1005 cm^{-1} frequency observed in the IR absorption experiments [64].

Table 2: Formation and binding energies of neutral interstitial oxygen complexes.

Complex	E_f	E_f/N_O	O_{ni} vs. nO_i	O_{ni} vs. $O_{(n-1)i}$ & O_i
O_i	1.1	1.1	-	-
O_{2i}	2.0	1.0	0.2	0.2
O_{3i}	2.8	0.9	0.5	0.3
O_{4i}	3.3	0.8	1.1	0.6
O_{5i}	3.8	0.8	1.7	0.6

3.4 Structures of thermal double donors in silicon

When Czochralski-grown Si crystal is annealed at 300-550°C thermal donors form. Thermal donors were first observed over 40 years ago [4] and since then they have been studied extensively [65–69]. Thermal donors have been found to consist of TDDs and single donors called shallow thermal donors (STD). In addition, at higher annealing temperatures a third family of donors, with a continuous distribution of energy levels is formed [70]. In 1978 two different thermal donors were detected with EPR. They were named NL8 and NL10 (the former being the donor considered here) [71]. Later it was found that both NL8 and NL10 consist of a series of donors. Recently, NL10 was shown to contain hydrogen or aluminum in the core and to be related to the STD [72]. The NL8 defect signal was found to consist of several TDDs, evolving with time. Subsequently, up to 17 TDDs have been observed [5, 73, 74]. The (0/+) and (+/++) levels of TDD0 are around $E_c - 0.07$eV and $E_c - 0.15$eV, respectively and they shift upwards with increasing TDD number [5, 65, 75]. The main contribution to NL8 comes from TDD3. Both EPR and electron nuclear double resonance (ENDOR) measurements require high concentration of donors and thus long annealing times. Long anneals destroy early donors (TDD0-TDD2) and thus these experiments give information only on TDDn's, n>2. The symmetry of TDD3 was deduced to be orthorhombic-I or C_{2v} with possible small deviations [65, 76–78]. Thus the defect has two symmetry (110) planes and a <001> symmetry axis. Measurements with oxygen isotope 17 showed that oxygen atoms lie in one (110) plane, and that no oxygen atoms are on the C_2 axis [77, 78]. TDDs are believed to have a common core into which oxygen atoms are added in the (110) plane. To maintain the C_{2v} symmetry, oxygen atoms are to be added in pairs to the TDD core. If the O atoms

are added one by one, then the symmetry should alternate between C_{1h} and C_{2v} [76].

Early TDDs (TDD0-TDD2) exhibit bistability: they have electrically neutral counterparts (X states) [5, 65, 75, 76]. TDDs and X states form a negative-U-system with the levels at $E_c - 0.32$eV and at $E_c - 0.22$eV [5] for TDD1 and TDD2, respectively. The X states can be frozen-in, if the crystal is cooled in darkness from room temperature to the temperatures where structural transformations are not possible [5].

Figure 7: The calculated three-oxygen structures, a) O_i-O_{2r}, b) Staggered O_{3i}.

The calculated O_i-O_{2r} structure shown in Fig. 7(a) consists of one O_i and one four-membered ring (two oxygen atoms - both denoted by O_r - bonded to two common Si atoms). This structure was originally proposed by Snyder and Corbett [79]. Chadi obtained a C_{2v} symmetric configuration with an O atom on the C_2 axis. He also found that small deviations from the perfect C_{2v} symmetry lower the total energy by 0.07 eV [67]. In Publication V it is also found that this C_{2v} symmetric configuration is unstable and relaxes to a structure shown in Fig. 7(a) in agreement with Ramamoorthy and Pantelides [69]. O_i-O_{2r} has an electronic state near the conduction band and it is thus a thermal donor. O_i-O_{2r} has a bistable electrically inactive configuration shown in Fig. 7(b) which is formed from O_i-O_{2r} by shifting one Si atom in the (110) plane. Since O_i-O_{2r} has the lowest energy of three-oxygen chains, it is assigned to TDD0.

Adding one oxygen atom to the O_i-O_{2r} structure results in O_i-O_{2r}-O_i shown in Fig. 8(a), or a more asymmetric O_{2i}-O_{2r} structure [Fig. 8(b)]. These both have a donor level near the conduction band minimum (See the insert in Fig. 10 below). O_i-O_{2r}-O_i and O_{2i}-O_{2r} have a common bistable electrically inert O_{4i} configuration shown in Fig. 8(c). Åberg *et al.* studied the TDD formation process using kinetic models based on IR absorption data [64]. They found that TDD2 could be formed from TDD1 via reconfiguration by migration of a single O_i. The calculated barrier between O_{2i}-O_{2r} and O_i-O_{2r}-O_i is low, equal to 0.36 eV. O_{2i}-O_{2r} and O_i-O_{2r}-O_i are assigned to TDD1 and TDD2, respectively.

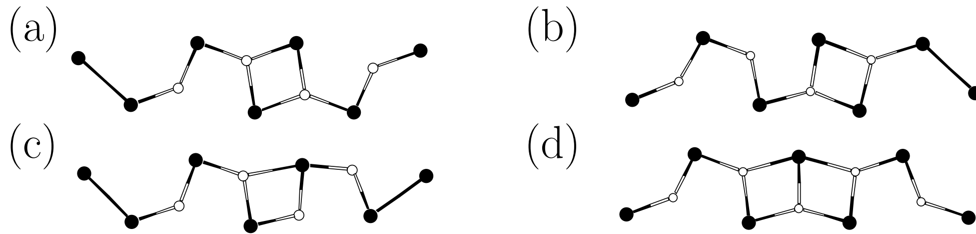

Figure 8: a) O_i-O_{2r}-O_i, b) O_{2i}-O_{2r}, c) Staggered O_{4i}, d) O_i-O_{nr}-O_i, n=3.

Adding more oxygen atoms to the O_4 chain results in a series of O_i-O_{nr}-O_i donors, n=3-8 having the alternating C_{2v}-C_{1h} symmetry: the chains with an even number of oxygen atoms have the symmetry of C_{1h}, those with an odd number the symmetry C_{2v}, in agreement with the experimental information on TDDs [65, 76–78]. However, the O_i-O_{nr}-O_i structures (n=3-8) have one oxygen atom on the C_2 axis. Since ENDOR and EPR experiments do not always detect light elements on the C_2 axis of a defect [80] and O_i-O_{nr}-O_i (n=3-7) are found to be the most stable among the possible candidates of donors including 5 - 9 O atoms, they are identified as TDD3-TDD7, respectively.

One of the oldest and most popular models for the TDD cores is the so-called di-Y-lid configuration [O_i-O_{2Y}-O_i, shown in Fig. 9(a)]. One reason for its popularity is the C_{2v} symmetry without any O atom on the C_2 axis. In Publication V it is found that the formation of the Si-Si bond drops the donor level from the E_c so that actually O_i-O_{2Y}-O_i is a deep donor. Moreover, the formation energy of O_i-O_{2Y}-O_i is more than 0.6 eV higher than that of O_i-O_{2r}-O_i and O_{2i}-O_{2r}.

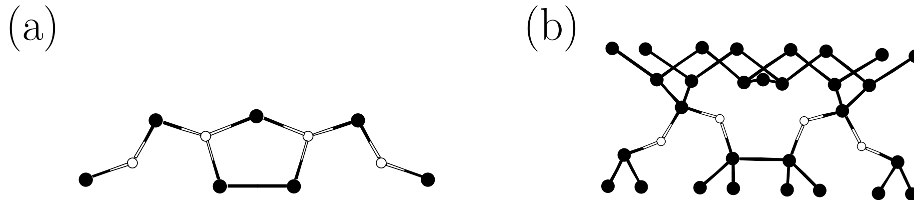

Figure 9: The calculated di-Y-lid configuration O_i-O_{2Y}-O_i a) (++), b) Neutral configuration derived from O_i-O_{2Y}-O_i configuration.

The calculated formation energies per oxygen atom and the Kohn-Sham donor levels are given in Fig. 10. The formation energy per oxygen atom of

the ring structures saturates to the value of 0.4 eV, while that of the di-Y-lid structures steadily decreases when $N_o \leq 10$. This is due to the larger ability of the di-Y-lid core to deform and release the strain caused by oxygen. The decrease leads to a crossover at 10 oxygen atoms, after which the di-Y-lid structures are energetically more favorable. The di-Y-lid structure has a stable configuration shown in Fig. 9(b) in which the silicon atom - crucial to obtain threefold coordinated oxygens - is shifted in the <001> direction near to the T_d interstitial site. This breaks the Si-O bonds and removes the donor character of the defect. The Si atom at the T_d interstitial site is not as strongly bonded to the oxygen chain as in the original three-valent position. The ejection of I from the oxygen chains $N_o \geq 10$ leads to the increase in I concentration, which has also been observed in experiments [81].

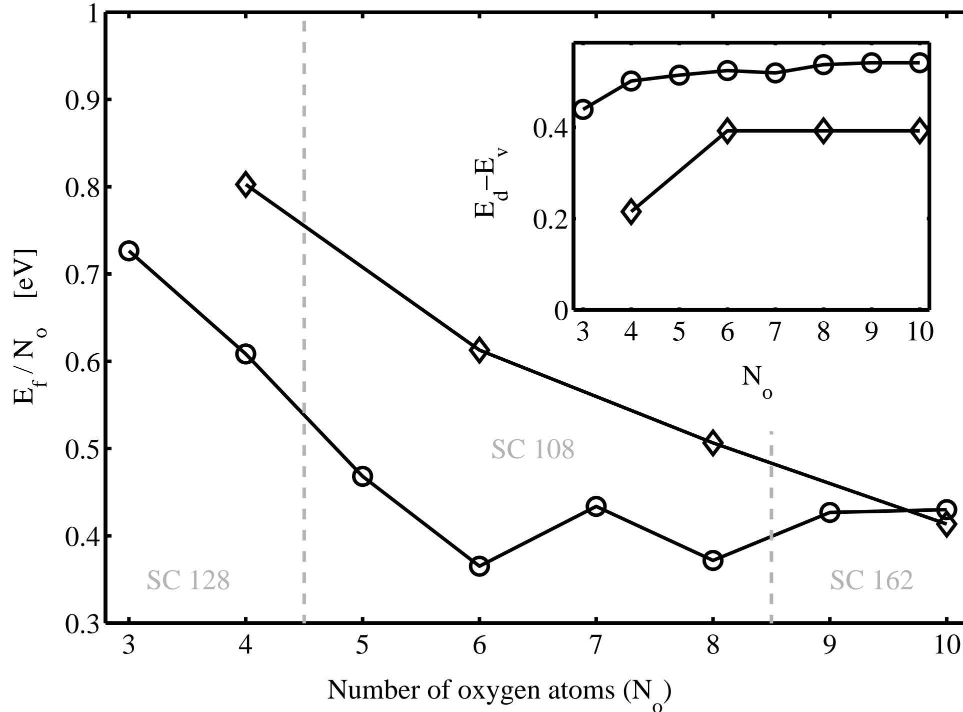

Figure 10: Formation energy per oxygen atom. Insert: behaviour of donor level position as a function of the number of oxygen atoms. Rings and diamonds denote ring and di-Y-lid structures, respectively.

Further evidence on behalf of ring structures is given by the behaviour of the Kohn-Sham donor levels as a function of the number of oxygen atoms

in the TDD (see the insert of Fig. 10). As observed in IR absorption measurements [5, 73, 74, 76] the donor level approaches similarly the conduction band minimum with increasing TDD number.

3.5 Oxygen-related defects in GaAs

In LEC-grown GaAs isolated oxygen impurities occur in the interstitial (Ga-O-As defect) and in the off-center substitutional (Ga-O-Ga defect) positions. A specific feature for the GaAs IR spectroscopy is the fine structure of the LVM bands due to the natural isotopes of Ga: ^{69}Ga and ^{71}Ga with the abundances of 60 % and 40 %, respectively. Therefore the Ga-O-As defect gives rise to a LV frequency doublet at 845 cm^{-1}, corresponding to two different Ga isotopes [82]. As in Cz-Si, interstitial oxygen in GaAs is electrically inactive. Another set of LV frequencies are detected at 731 and 715 cm^{-1} (denoted by A and B, respectively) [83]. These frequencies show a characteristic triplet fine structure caused by the Ga isotopes [83, 84]. From the observed ^{18}O$\rightarrow$ ^{16}O isotopic shifts in LV frequencies it has been concluded that oxygen is involved in this defect [82] and thus the frequencies originate from a Ga-O-Ga structure. The LV frequencies show photosensitivity: in semi-insulating (SI) GaAs the band A can be converted by illumination into the band B via a third band B' located 0.7 cm^{-1} below B [83,85,86]. A, B', and B are zero-, one-, and two-electron states of the Ga-O-Ga defect, respectively [85]. The Ga-O-Ga defect exhibits a negative-U property [85], B' being a metastable paramagnetic state [87]. The ionization levels are 0.15 (level filled by one electron) and 0.62 eV (level filled by two electrons) below the conduction band [85].

In Publication VI the origin of these LV frequencies in GaAs were studied. The assumed similarity between oxygen-related defects in Si and GaAs has led to a proposition that the microscopic structure of the Ga-O-Ga defect is similar to the A center in Si. In Publication VI it was shown that the properties of this model, O_{As} (an off-centered substitutional oxygen in arsenic vacancy) are inconsistent with experimental data.

Recently, Taguchi and Kageshima [88] suggested that an interstitial oxygen near the T_d position (denoted by O_I) is the Ga-O-Ga defect. In their calculations O is bonded to two Ga atoms and therefore this structure could give the LV modes and frequencies similar to the experimentally observed ones. In Publication VI it was shown that the oxygen atom near the T_d position is bonded to three or four Ga atoms depending on the charge state

Table 3: Properties of defects having oxygen in substitutional off-centered position.

Complex	'A'	'B'	defect state
Calculations			
VO in Si	843	850	antibonding
O_{As}	648	705	antibonding
$(As_{Ga})_2$-O_{As}	748	738	bonding
Experiments			
VO in Si	835	885	antibonding
Ga-O-Ga	730	715	-

of the defect. Furthermore, it was shown that the Ga-O-As defect is more than 1 eV lower in energy than O_I, thus rejecting the model. The Ga-O-As defect occupies a similar bond-centered structure as interstitial oxygen in Si. The calculated asymmetric stretching frequency of Ga-O-As is calculated to be 869 cm^{-1}, in close agreement with the experimental value of 845 cm^{-1}.

In Publication VI also a new structure for the Ga-O-Ga defect is introduced. It exhibits a strong negative-U character as well as LV frequencies in agreement with the experimental values. This structure consists of two arsenic antisites and one substitutional oxygen [$(As_{Ga})_2$-O_{As}].

One of the strongest points on behalf of $(As_{Ga})_2$-O_{As} is based on a simple tight-binding argument. Figure 11(a) shows a tight-binding model for $(As_{Ga})_2$-O_{As}. The downwards shift in the LV frequency A→B induced by charging originates from the bonding nature of the defect state in the forbidden energy gap. In Table 3, the antibonding - bonding character and the LV frequencies of some defects are listed. Similarity between O_{As} and VO in Si is apparent: filling the defect level of antibonding nature leads to an increase in the LV frequencies. The defect level and the corresponding wavefunction of $(As_{Ga})_2$-O_{As} is of bonding nature and its occupation changes the structure of the defect in such a way that the LV frequency shifts downwards. Figure 11(b) shows this bonding Kohn-Sham electronic state of the defect in the plane containing the As_{Ga}s and the oxygen atom.

Other studied structures include As_{Ga}-O_{As} and Ga_{As}-O_i. Table 4 shows the calculated formation energies for these and also for some relevant native

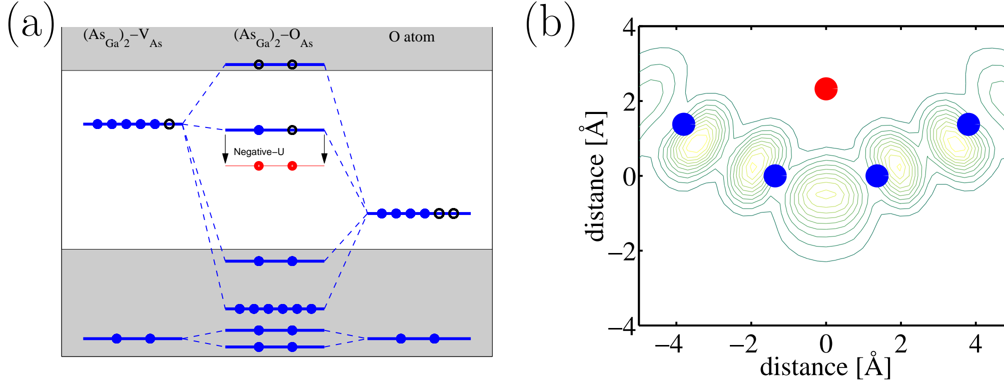

Figure 11: a) Schematic tight-binding diagram for $(As_{Ga})_2$-O_{As}. The negative-U effect is seen in the Kohn-Sham eigenvalue of the defect level. b) The uppermost occupied electronic state in the plane containing arsenic antisites and oxygen atom. The defect state occupied by one electron in the neutral charge state is of the bonding type between the two As_{Ga} defects.

defects.

The driving force in the defect complex formation is the Coulomb interaction between the constituents of the defect. Oppositely charged defects feel mutual interaction, while there is an electrostatic barrier to overcome for similarly charged defects.

Another contributing factor is the concentration of the defects. In SI GaAs there are more V_{Ga} than V_{As} defects. It is also known that SI GaAs contains EL2 defects about 10^{16} 1/cm^3 [89]. The EL2 defects have a (++/0) level in the band gap and they are thought to be arsenic antisites. The $(As_{Ga})_2$-O_{As} model contains two As_{Ga}s and therefore the EL2 defect related closely to As_{Ga} may be an essential part of the Ga-O-Ga defect.

When the Fermi level is in the mid-gap, the thermodynamically stable charge state of the V_{Ga} is trebly negative. Therefore the formation of the As_{Ga}-V_{Ga} complex is facilitated by Coulomb attraction between it and the positively charged As_{Ga}. V_{Ga} is known to be metastable with the competing V_{As}-As_{Ga} structure [36]. This leads to a possibility of a defect $(As_{Ga})_2$-V_{As} which is a native defect missing only an oxygen atom to form the needed $(As_{Ga})_2$-O_{As} model of the Ga-O-Ga defect. In the As-rich GaAs the formation energy of $(As_{Ga})_2$-V_{As} is lower than the formation energy of V_{As} (See Table 4).

Table 4: Formation and binding energies of neutral interstitial oxygen complexes in As-rich GaAs. All calculations are done with the same 32 atom-site supercell and MP **k**-point sampling. In the case of charged defects the electron chemical potential is set to be in the midgap ($\mu_e = E_g/2$).

Complex	E_f (eV)
As_{Ga}	1.7
V_{Ga}^-	2.1
$(As_{Ga})_2$-V_{As}	3.4
V_{As}	3.8
Ga-O-As	3.2
O_{As}^-	3.2
$[As_{Ga}$-$O_{As}]^-$	3.5
$[(As_{Ga})_2$-$O_{As}]^-$	3.9
O_I	4.7

Early studies by Watkins and Corbett showed that the A center reorients with a barrier of 0.38 eV when uniaxial stress is applied to the Si crystal [12]. However, Song *et al.* [90] concluded based on their piezospectroscopic measurements that the Ga-O-Ga defect does not exhibit such a behaviour. Structurally both O_{As} and O_I have no mechanism which would hinder their reorientation. The presence of two As_{Ga}s in the $(As_{Ga})_2$-O_{As} model explains the absence of reorientation in a natural way.

4 Summary

In this thesis vacancies and oxygen-related point and extended defects in Si and GaAs have been studied.

The plane-wave pseudopotential (PWPP) calculations give reliable electronic and structural information about defects in semiconductors. It has been shown that using calculated defect formation energies and local vibrations, defects can be efficiently identified. PWPP calculations are thus a powerful method with a predictive power.

In Publications I and II the convergence of electronic structure calculations with respect to supercell size and **k**-point sampling in the case of vacancies in Si were studied. It was shown that although the energies are converged, obtaining convergence in the ionic structures requires large supercells.

Publication III contained a systematic study of VO complexes and small interstitial oxygen complexes. The calculated properties of oxygen-related defects were shown to be in agreement with the experiments. Especially the ionization levels and local vibrational modes and frequencies are obtained with reasonable accuracy.

Publication IV utilizes the information obtained in Publication III and applies it to oxygen dimers in silicon. With the help of calculated local vibrational frequencies the IR frequencies were assigned to the staggered configuration of the oxygen dimer.

Publication V is the first electronic structure study of oxygen clusters containing more than five oxygen atoms. The formation energy differences between two competing oxygen-only structures were considered. First three TDDs were assigned to structures consisting of one four-member ring, containing two three-fold coordinated O atoms responsible for the donor property and one or two adjacent interstitial O atoms. TDD3-TDD7 were assigned to structures consisting of more adjacent four-member rings with interstitial O atoms at the ends. The chains with a central di-Y-lid core were found to become energetically competitive with the four-member ring structures at ten O atoms.

In Publication VI the structure of the Ga-O-Ga defect in GaAs was shown to be $(\mathrm{As_{Ga}})_2$-$\mathrm{O_{As}}$. This defect exhibits the negative-U phenomenon and charge-state-induced shifts in local vibrational modes, in agreement with the experiments.

References

[1] P. Wagner, J. Hage, J. M. Trombetta, and G. D. Watkins, Mat. Sci. Forum Vols. **83-87**, p. 401 (1992).

[2] R. C. Newman, in *Early Stages of Oxygen Precipitation in Silicon*, edited by R. Jones (Kluwer Academic Publishers, Dordrecht, 1996) p. 19.

[3] L. I. Murin, T. Hallberg, V. P. Markevich, and J. L. Lindström, Phys. Rev. Let. **80**, 93 (1998).

[4] C. S. Fuller, J. A. Ditzenberger, N. B. Hannay, and E. Buehler, Phys. Rev. **96**, 833 (1954).

[5] P. Wagner and J. Hage, Appl. Phys. A**49**, 123 (1989).

[6] H. Navarro, J. Griffin, J. Weber, and L. Genzel, Solid State Communications **58**, 151 (1986).

[7] W. Cazcarra and P. Zunino, J. Appl. Phys. **51**, 4206 (1980).

[8] G. D. Watkins and J. R. Troxell, Phys. Rev. Lett **44**, 593 (1980); J. R. Troxell and G. D. Watkins, Phys. Rev. B **22**, 921 (1980).

[9] G. D. Watkins and J. W. Corbett, Phys. Rev. **138**, A543 (1965).

[10] M. Saito and A. Oshiyama, Phys. Rev. Lett. **73**, 866 (1994).

[11] G. D. Watkins, J. W. Corbett, and R. M. Walker, J. Appl. Phys. **30**, 1198 (1959).

[12] G. D. Watkins and J. W. Corbett, Phys. Rev. **121**, 1001 (1961).

[13] P. Hohenberg and W. Kohn, Phys. Rev. **136**, B864 (1964).

[14] W. Kohn and L. J. Sham, Phys. Rev. **140**, A1133 (1965).

[15] H. Hellmann, *Einführung in die Quantenchemie*, (Deuticke, Leipzig, 1937); R. P Feynman, Phys. Rev. **56**, 340 (1939); See, e.g., L. D. Landau and E. M. Lifshitz, *Quantum Mechanics - Non-relativistic Theory*, 3rd edition (Pergamon, Oxford, 1977), p. 34.

[16] O. Gunnarsson and B. I. Lundqvist, Phys. Rev. B **13**, 4274 (1976).

[17] D. M. Ceperley and B. J. Alder, Phys. Rev. Lett. **45**, 566 (1980).

[18] J. Perdew and A. Zunger, Phys. Rev. B **23**, 5048 (1981).

[19] S. H. Vosko, L. Wilk and M. Nusair, J. Can. Phys. **58**, 1200 (1980).

[20] See, e.g., J. P. Perdew in *Electronic Structure of Solids '91*, edited by P. Ziesche and H, Eschrig (Akademie-Verlag, Berlin, 1991).

[21] G. E. Engel and W. E. Pickett, Phys. Rev. B **54**, 8420 (1996).

[22] A. Seidl, A. Görling, P. Vogl, J. A. Majevski, and M. Levy, Phys. Rev. B **53**, 3764 (1996).

[23] D. J. Chadi and K. J. Chang, Phys. Rev. Lett. **60**, 2187 (1988).

[24] W. C. Topp and J. J. Hopfield, Phys. Rev. B **7**, 1295 (1973).

[25] D. R. Hamann, M. Schlüter, and C. Chiang, Phys. Rev. B **43**, 1494 (1979).

[26] G. B. Bachelet, D. R. Hamann, and M. Schlüter, Phys. Rev. B **26**, 4199 (1982).

[27] D. R. Hamann, Phys. Rev. B **40**, 2980 (1989).

[28] D. Vanderbilt, Phys. Rev. B **41**, 7892 (1990); K. Laasonen, A. Pasquarello, R. Car, C. Lee, and D. Vanderbilt, Phys. Rev. B **47**, 10142 (1993).

[29] H. J. Monkhorst and J. D. Pack, Phys. Rev. B **13**, 5188 (1976).

[30] G. Makov, R. Shah, and M. C. Payne, Phys. Rev. B **53**, 15 513 (1996).

[31] G. Makov and M. C. Payne, Phys. Rev. B **51**, 4014 (1995).

[32] J. Lento, M. Pesola, J.-L. Mozos, and R. M. Nieminen, Accepted for publication in Applied Physics Letters.

[33] G. -X. Qian, R. M. Martin, and D. J. Chadi, Phys. Rev. B **38**, 7649 (1988).

[34] S. B. Zhang and J. E. Northrup, Phys. Rev. Lett **67**, 2339 (1991).

[35] T. Mattila and R. M. Nieminen, Phys. Rev. B **54**, 16676 (1996).

[36] S. Pöykkö, M. J. Puska and R. M. Nieminen, Phys. Rev. B **53**, 3813 (1996).

[37] Ville Sammalkorpi, private communication.

[38] Th. Köhler, Th. Frauenheim and G. Jungnickel, Phys. Rev. B **52**, 11837 (1995).

[39] M. C. Payne, M. P. Teter, D. C. Allan, T. A. Arias, and J. D. Joannopoulos, Rev. Mod. Phys. **64**, 1045 (1992).

[40] J. Hubbard, Proc. Roy. Soc. London Ser. A **276**, 238 (1963).

[41] P. W. Anderson, Phys. REv. Lett. **34**, 953 (1975).

[42] S. T. Pantelides, in *Deep centers in semiconductors*, edited by S. T. Pantelides (Gordon and Breach Science Publishers, 1986).

[43] G. A. Baraff, E. O. Kane, and M. Schlüter, Phys. Rev. B **21**, 5662 (1980).

[44] S. Öğüt, H. Kim, and J. R. Chelikowsky Phys. Rev. B **56**, R11 353 (1997).

[45] J. W. Corbett and J. C. Bourgoin in *Point Defects in Solids, vol. 2*, edited by J. H. Crawford and L. M. Slifkin (Plenum Press, New York, 1974).

[46] S. Öğüt and J. R. Chelikowsky, Phys. Rev. Lett. **83**, 3852 (1999).

[47] G. D. Watkins, Phys. Rev. B **12**, 5824 (1975).

[48] G. K. Wertheim, Phys. Rev. **105** 1730 (1957).

[49] G. K. Wertheim, Phys. Rev. **110** 1272 (1958).

[50] D. E. Hill, Phys. Rev. **114** 1414 (1959).

[51] J. L. Lindström and B. G. Svensson, Mat. Res. Soc. Symp. Proc. **59**, 45 (1986).

[52] J. W. Corbett, G. D. Watkins and R. S. McDonald, Phys. Rev. **135**, A1381 (1964).

[53] C. A. Londos, G. I. Georgiou, L. G. Fytros, and K. Papastergiou, Phys. Rev. B **50**, 11531 (1994).

[54] F. A. Abou-el-Fotouh and R. C. Newman, Solid State Commun. **15**, 1409 (1974).

[55] J. Svensson, B. G. Svensson, and J. L. Lindström, Appl. Phys. Lett. **49**, 1435 (1986).

[56] H. J. Stein, Mat. Sci. Forum Vols. **10-12**, p. 935 (1986).

[57] Y.-H. Lee and J. W. Corbett, Phys. Rev. B **13**, 2653 (1976).

[58] H. J. Hrostowski and R. H. Kaiser, Phys. Rev. **107**, 966 (1957).

[59] H. J. Hrostowski and B. J. Alder, J. Chem. Phys. **33**, 980 (1960).

[60] D. R. Bosomworth, W. Hayes, A. R. L. Spray, and G. D. Watkins, Proc. R. Soc. London Ser A **317**, 133 (1970).

[61] M. D. McCluskey and E. E. Haller, Phys. Rev. B **56**, 9520 (1997).

[62] S. Öberg, C. P. Ewels, R. Jones, T. Hallberg, J. L. Lindström, L. I. Murin, and P. R. Briddon, Phys. Rev. Lett. **81**, 2930 (1998).

[63] T. Hallberg, J. L. Lindström, L. I. Murin, and V. P. Markevich, Mat. Sci. Forum Vols. **258-263**, p. 361 (1997).

[64] D. Åberg, B. G. Svensson, T. Hallberg, and J. L. Lindström, Phys. Rev. B **58**, 12944 (1998).

[65] *Early Stages of Oxygen Precipitation in Silicon*, edited by R. Jones (Kluwer Academic Publishers, Dordrecht, 1996) and references therein.

[66] M. Needels, J. D. Joannopoulos, Y. Bar-Yam, and S. T. Pantelides, Phys. Rev. B **43**, 4208 (1991).

[67] D. J. Chadi, Phys. Rev. Lett. **77**, 861 (1996).

[68] P. Deák, L. C. Snyder, and J. W. Corbett, Phys. Rev. B **45**, 11612 (1992).

[69] M. Ramamoorthy and S. Pantelides, Appl. Phys. Lett. **75**, 115 (1999).

[70] G. Pensl, M. Schulz, K.Hölzlein, W. Bergholz, and J. L. Hutchison, Appl. Phys. A: Solids Surf. **48**, 49 (1989).

[71] S. Muller, M. Sprenger, E. G. Sievert, and C. A. J. Ammerlaan, Solid State Communications **25**, 987 (1978).

[72] R. C. Newman, J. H. Tucker, N. G. Semaltianos, E. C. Lightowlers, T. Gregorkiewicz, I. S. Zevenbergen, and C. A. J. Ammerlaan Phys. Rev. B**54**, R6803 (1996).

[73] B. Pajot, H. Complain, J. Lerouille, and B. Clerjand, Physica **117 & 118 B**, 110 (1983).

[74] W. Götz, G. Pensl, and W. Zulehner, Phys. Rev. B **46**, 4312 (1992).

[75] Ya. I. Latushko, L. F. Makarenko, V. P. Markevich, and L. I. Murin, Phys. Stat. Sol. (a) **93**, K181 (1986).

[76] C. A. J. Ammerlaan in *Properties of Crystalline Silicon*, edited by R. Hull (INSPEC, London, 1999), p. 663.

[77] J. Michel, J. R. Niklas, and J. -M. Spaeth, Phys. Rev. B **40**, 1732 (1989).

[78] T. Gregorkiewicz, H. H. P. Th. Bekman, and C. A. J. Ammerlaan, Phys. Rev. B **41**, 12628 (1990).

[79] L. C. Snyder and J. W. Corbett, in *Oxygen, Carbon, Hydrogen and Nitrogen in Crystalline Silicon*, edited by J. C. Mikkelsen, Jr., S. J. Pearton, J. W. Corbett, and S. J. Pennycook, Mat. Res. Soc. Symp. Proc. **59**, 207 (1986).

[80] G. Davies and R. C. Newman, in *Handbook on Semiconductors*, edited by T. S. Moss (Elsevier Science BC, 1994).

[81] R. C. Newman, A. S. Oates, and S. M. Livingston, J. Phys. C **16**, L667 (1983).

[82] J. Schneider, B. Dischler, H. Seelewind, P. M. Mooney, J. Lagowski, M. Matsui, D. R. Beard, and R. C. Newman, Appl. Phys. Lett. **54**, 1442 (1989).

[83] C. Song, W. Ge, D. Jiang, and C. Hsu, Appl. Phys. Lett. **50**, 1666 (1987).

[84] X. Zhong, D. Jiang, W. Ge, and C. Song, Appl. Phys. Lett. **52**, 628 (1988).

[85] H. Ch. Alt, Appl. Phys. Lett. **54**, 1445 (1989); **55**, 2736 (1989); Phys. Rev. Lett. **65**, 3421 (1990).

[86] C. Song, B. Pajot, and F. Gendron, J. Appl. Phys. **67**, 7307 (1990).

[87] M. Linde, J.-M. Spaeth, and H. Ch. Alt, Appl. Phys. Lett.**67**, 662 (1995).

[88] A. Taguchi and H. Kageshima, Phys. Rev. B **57**, R6779 (1998).

[89] D. E. Holmes, R. T. Chen, K. R. Elliot, and G. G. Kirkpatrick, Appl. Phys. Lett. **40**. 46 (1982).

[90] C. Song, B. Pajot, and C. Porte, Phys. Rev. B **41**, 12330 (1990).